NASA CR 135360
PWA-5590

AN ANALYTICAL STUDY OF THERMAL BARRIER COATED FIRST STAGE BLADES IN A JT9D ENGINE

By
William R. Sevcik and Barry L. Stoner

United Technologies Corporation
Pratt & Whitney Aircraft Group
Commercial Products Division

Prepared for
National Aeronautics and Space Administration

NASA Lewis Research Center
Contract NAS3-21033

1 Report No.	2 Government Accession No	3 Recipient's Catalog No.
NASA CR-135360		

4 Title and Subtitle	5 Report Date
An Analytical Study of Thermal Barrier Coated First Stage Blades in a JT9D Engine	January 1978
	6 Performing Organization Code

7 Author(s)	8 Performing Organization Report No.
William R. Sevcik and Barry L. Stoner	PWA-5590
	10 Work Unit No

9 Performing Organization Name and Address	11 Contract or Grant No
Commercial Products Division Pratt & Whitney Aircraft Group United Technologies Corporation - East Hartford, CT 06108	NAS3-21033
	13 Type of Report and Period Covered

12 Sponsoring Agency Name and Address	13 Type of Report and Period Covered
	Contractor Report
National Aeronautics and Space Administration Washington, D. C. 20546	14 Sponsoring Agency Code

15 Supplementary Notes

Mr. John P. Merutka, Project Manager
NASA Lewis Research Center, Cleveland, Ohio 44135

16 Abstract

An analytical study was conducted to evaluate the thermal barrier coating on first stage turbine blades that were endurance tested in a JT9D engine. Steady state and transient heat transfer and structural calculations were completed to determine the coating and base alloy temperatures and strains. Results indicate potential for increased turbine life using thin durable thermal barrier coatings on turbine airfoils due to a significant reduction in blade average and maximum temperatures, and alloy strain range. An intepretation of the analytical results is compared to the experimental engine test data.

17 Key Words (Suggested by Author(s))	18 Distribution Statement
Thermal Barrier Coating Turbine Blades JT9D Engine Test Thermal and Structural Analysis	

19 Security Classif. (of this report)	20 Security Classif. (of this page)	21 No. of Pages	22 Price*
Unclassified	Unclassified	32	

* For sale by the National Technical Information Service, Springfield, Virginia 22151

TABLE OF CONTENTS

LIST OF ILLUSTRATIONS

1.0 INTRODUCTION

A JT9D-7F engine endurance test was conducted to assess the durability of both the NASA (Reference 1) applied and the P&WA applied thermal barrier coatings on the first stage turbine blades. Six NASA coated blades and five P&WA blades were tested. This test recorded 264 total engine hours, of which 190 hours were endurance hours accumulating 1424 thermal cycles. A typical thermal cycle was composed of 2 minutes at take-off power and 5 minutes at idle power with maximum turbine inlet temperatures reaching 2600°F.

Limited success was obtained with P&WA and NASA plasma sprayed two-layered NiCoCrAlY or NiCrAlY plus yttria stabilized zirconia thermal barrier coating systems which were applied over an oxidation resistant PWA 270 coating.

After 39 hours (327 cycles) of operation in experimental engine X-493-27A, coating failures were observed only at the leading edge (highest temperature) locations. An additional 225 hours (1097) cycles of operation in experimental engine build X-579-12, 12A, 13, 13A partially spalled about one third of the thermal barrier coatings on the pressure (concave) side of the airfoils near the 70% span. Visual examination indicated that the thermal barrier coatings were unfailed at other locations on the airfoils and the platforms after the total of 264 hours (1424 cycles) of engine testing.

Following these engine tests it was proposed that a design analysis be conducted to evaluate the thermal barrier coated blade results.

The objectives of this program were to conduct a heat transfer analysis and a structural analysis of a NASA thermal barrier coated JT9D-7F first stage turbine blade tested in experimental engine X-579 and provide an interpretation of the analytical results.

2.0 CONCLUSIONS

1. The use of thin durable thermal barrier coatings on the JT9D first stage turbine blades with the same coolant provides the potential for a significant increase in turbine life because of the large reduction in blade average metal temperature, maximum metal temperature, and strain range.

2. The thermal barrier coating failures observed on the first stage turbine blades tested in the JT9D-7 engines (X-493 and X-579) occurred at the regions of highest blade temperatures.

3. Since ceramic coating failures did not occur in all regions of high strain, other failure mechanisms associated with the high temperature must be present.

4. The thermal barrier coating did fail in regions where the compressive strains were greatest, i.e. the leading edge and the pressure wall.

3.0 RECOMMENDATIONS

1. The ceramic temperatures on the JT9D blades often exceeded the brittle-ductile transition temperature range (see Figure 17) above which effects of creep, sintering shrinkage, etc. are accelerated. These high temperature effects were not studied in this elastic analysis and should be evaluated as possible modes of failure.

2. An experimentally determined failure criterion, that of ceramic rupture strain based on limited four point bending test data, was used for this anlysis. Other failure criteria related to compressive buckling, erosion, and creep should be identified and suitable test data should be measured to establish the necessary coating durability design criteria.

3. The stress free temperature controlled application process needs further study and experimental effort to determine its effect on improving coating durability.

4.0 DESCRIPTION OF ANALYSIS

The JT9D-7F first stage turbine blade was evaluated during both transient and steady state engine conditions.

The thermodynamic boundary conditions and the centrifugal loading used for the analysis reflect the operation of the JT9D-7 experimental engines (X579-12, X-493-27A) during a snap accel-decel engine cycle, ref. Figure 1.

A two-dimensional finite element blade model was used with the computer to conduct the heat transfer analysis and the stress analysis. This model was prepared using appropriate material properties for the coating layers and base alloy presented in the Appendix.

The thermal barrier coating for the NASA prepared airfoil consisted of a seven mils thick layer of yttria stabilized zirconia ($Y_2O_3ZrO_2$) and a three-mils thick bond layer of NiCrAlY. This ceramic coating was plasma sprayed over a base alloy of directionally solidified MARM 200 plus hafnium (PWA 1422) which was coated for oxidation protection with a thin vapor deposited NiCoCrAlY layer (PWA 270). The model consisted of five elemental layers through the coating/alloy system, using two elements for the ceramic, combining the bond layer and the vapor deposited layer into a single element, and using two elements for the base alloy.

The mechanical and thermal stress calculations were based on both in-plane and out-of-plane analyses. The in-plane elastic analysis was two-dimensional without centrifugal loading and the out-of-plane analysis was one-dimensional along the blade span including centrifugal loads. A three-dimensional equation was used to determine the elastic strain in the spanwise direction by coupling the results of the in-plane and out-of-plane analyses. This out-of-plane elastic strain ϵ_z was defined by

$$\epsilon_z = \frac{1}{E}[\sigma_z - \upsilon\,(\sigma_x + \sigma_y)]$$

where $E \equiv$ modulus of material

$\upsilon \equiv$ Poisson's ratio

$\sigma_{x,y,z} \equiv$ stresses from in-plane and out-of-plane analyses

The calculated strains were then used to determine the strain range for the coating and the base alloy. The strain range of a material element is defined as the maximum strain minus the minimum strain which occurs during an engine cycle.

The thermal and stress calculations were performed at two spanwise locations, 25% span and 70% span, which were selected because they represent both unfailed regions and failed regions of the test airfoils.

5.0 REFERENCE TEMPERATURE DISCUSSION

During the ceramic application process, the substrate temperature can increase several hundred degrees. When the ceramic and the substrate cool to room temperature, compressive stresses occur in the ceramic due to its lower coefficient of expansion. For the composite finite element stress analysis, all thermally induced stresses and strains must be calculated relative to a state of zero stress and strain. This zero stress condition is defined to occur when the ceramic - substrate interface is at the bonding temperature. Calculations based on this zero stress condition require that the reference temperature for the linear expansion coefficient, α, be the stress free temperature, not room temperature (RT), which is common for most materials.

The following equation can be used to generate an effective linear expansion coefficient, α_e, based on a reference stress free temperature.

$$\alpha_e = \frac{\alpha\,(T\text{-}70) - \alpha_{sf}\,(T_{sf}\text{-}70)}{(T\text{-}T_{sf})}$$

where α and α_{sf} are the linear expansion coefficients based on the reference room temperature and evaluated at T and T_{sf} (stress free temperature).

The stress free reference temperature used to calculate the ceramic strains for the thermal barrier coated JT9D first stage turbine blade was determined from laboratory testing conducted under IR&D funding at Pratt & Whitney Aircraft. This laboratory work measured the temperature of a sixty mils thick curved nickel alloy substrate during the application of a thermal barrier coating. This laboratory specimen was coated at an initial substrate temperature of 70°F which increased during the process of the plasma sprayed coating application (reference Figure 2). The JT9D blades have a nominal wall thickness which varies from 35 mils to 60 mils and were coated using a similar plasma spray process. The thermocouple in the laboratory specimen was embedded 25 mils below the surface. To determine the temperature of the bond layer which was defined as the stress free temperature during coating application, a calculation was performed to relate the stress free temperature to the thermocouple measurement of the substrate. The calculated stress free temperature based on the laboratory result was 700°F. The stress/strain results for the JT9D blade study were based on the 700°F stress free temperature.

Other laboratory data indicate that the stress free temperature is influenced by substrate thickness. Thinner substrate thicknesses resulted in higher stress free temperatures which could in turn result in higher compression upon cooling.

The stress analysis programs used for this study did not have the capability for applying different reference temperatures for each element, however, a separate calculation was performed assuming that the stress free temperature was at 500°F. One result presented in the appendix, reference Figure 12, indicates that, in general, the elemental strain range was unchanged although the elemental strains occurred at a different level of compression. This result suggests that stress and strain levels can be controlled if the level of the stress free temperature can be controlled.

6.0 HEAT TRANSFER RESULTS

The following figures present the temperature results for the thermal barrier coated blade analysis.

Figure 3 shows the element centroid temperatures through the composite layers at 25% span. A large temperature gradient is seen to occur across the ceramic for the Sea Level Takeoff (SLTO) operating condition. The average temperature gradient across the ceramic and substrate are 21.2°F/mil and 1.84°F/mil, respectively. The four regions shown were selected because the highest ceramic strains occurred at these locations.

Figure 4 shows the element centroid temperatures through the composite layers at 70% span and SLTO. The average gradients for ceramic and substrate are 26.0°F/mil and 2.17°F/mil, respectively. The temperature gradients for this hotter span location are more severe than at 25 % span.

Figure 5 shows the thermal barrier coated and uncoated average substrate temperatures for 25% and 70% span. The coated airfoil average metal temperature at the 25% span is 87°F less than uncoated blade average metal temperature and the coated airfoil average metal temperature at the 70% span is 98°F less than uncoated blade average metal temperature. The maximum blade metal temperature at the 70% span location is 120°F colder for the coated airfoil versus the uncoated airfoil. This maximum temperature occurs at the blade leading edge.

Figure 6 shows the temperature response of the multiple materials comprising the airfoil wall section relative to the cycle time during accel and decel. Also note the response of the blade environment gas temperature. Other boundary conditions are contained in the Appendix.

7.0 STRAIN AND STRESS RESULTS

This next series of results presents the strains for the two airfoil sections and a table of elastic stresses.

Figures 7 and 8 show the ceramic strain (outermost element) versus temperature at the four regions of highest strain (reference Figure 3) and for the two airfoil sections (25% span and 70% span).

Figures 9 and 10 show the ceramic strain (outermost element) versus cycle time at the four regions of highest strain and at the two airfoil sections.

The strains for the remaining composite layers (inner ceramic element, bond layer, base alloy) are shown in Figure 11 at the blade trailing edge pressure side, 70% span location. These strains may be compared with the ceramic surface element strains given in Figure 8.

The elastic stresses for the ceramic layer at the four regions of highest strain are given in Table I for both airfoil sections.

Another result of interest to the designer is the base alloy strain range for both thermal barrier coated airfoils and uncoated airfoils. These results are presented in Table II.

TABLE I

ELASTIC STRESSES FOR OUTER CERAMIC LAYER DURING STEADY STATE AND TRANSIENT OPERATION

25 PERCENT SPAN	SUCTION SIDE TRAILING EDGE	SUCTION SIDE MID-CHORD	LEADING EDGE	PRESSURE SIDE TRAILING EDGE
SLTO	σ_{MAX} ~ KSI	9 15	9 16	4 48	5 83
	TEMP ~ °F	1852	1885	1954.	1902
DECEL	σ_{MAX} ~ KSI	16 47	17 85	12 77	15 36
T = 2.0 SEC	TEM ~ F	1362	1432	1234	1311
ACCEL	σ_{MAX} ~ KSI	6 48	6 88	-17.28	-9 05
T = 1.2 SEC	TEMP ~ °F	1155	1133	1405.	1247
70 PERCENT SPAN	SUCTION SIDE TRAILING EDGE	SUCTION-SIDE MID-CHORD	LEADING EDGE	PRESSURE SIDE TRAILING EDGE
SLTO	σ_{MAX} ~ KSI	4 32	4 82	3 57	2 26
	TEMP ~ °F	1991	1998	2107.	2026.
DECEL	σ_{MAX} ~ KSI	14 89	14.39	11 30	12.28
T = 2.0 SEC	TEMP ~ °F	1412	1522	1357	1392
ACCEL	σ_{MAX} ~ KSI	10 35	9 33	-18 44	10.55
T = 1.2 SEC	TEMP ~ °F	1300	1201	1510	1332.

TABLE II

BASE ALLOY STRAIN RANGE FOR COATED AND UNCOATED AIRFOIL
RESULTS AT 70% SPAN LOCATION (IN./IN.)

70 PERCENT SPAN	LEADING EDGE	SUCTION SIDE	SUCTION SIZE TRAILING EDGE	PRESSURE SIZE TRAILING EDGE
COATED	.0026	.0008	.0008	.0004
UNCOATED	.0032	.0011	.0011	.0012

8.0 DISCUSSION OF RESULTS

The hottest calculated airfoil temperatures occurred at the 70% blade span location. These temperatures were approximately 100°F hotter than the 25% span location. Considering the four airfoil regions where the ceramic strain range was calculated to be large, the leading edge 70% span region - where the ceramic failure occurred first in X-493 - was calculated to have the highest temperature and the highest strain range. Comparing the temperature and strain range levels of the other regions, the pressure side (70% span) trailing edge region had the second highest temperature level but not the second highest strain range. The experimental hardware subsequently tested in X-493 and X-579 resulted in failure on the pressure wall as well as the leading edge. Although the suction side (70% span) was calculated to have high strain range elements, the experimental hardware did not indicate failure on the airfoil suction wall. Therefore, the conclusion drawn is that the ceramic coating failures correlate best with temperature level. Failure mechanisms associated with temperature level suggest failure modes of creep, sintering, or oxidation volumetric expansion. These modes were discussed in an informal report to NASA (reference 2).

Another difference between the 25% span and the 70% span was that the ceramic layer had less compression at the 25% span because of the higher centrifugal loading. In the regions where coating failure did occur, the ceramic surface layer was calculated to have the greatest compressive strains. As mentioned previously, the thinner blade walls near the trailing edge could have resulted in a higher stress free temperature in that region and also increased the compression strains.

The stress analysis conducted for this study was an elastic analysis from which stresses and strains due to mechanical and thermal loading were evaluated. Although a one to one relation cannot be established between observed failure and strain, it is believed that high ceramic strains contribute to the failures.

The strain ranges for the inner element ceramic layer, the bond layer and the substrate elements are calculated to be small when compared to the surface layer ceramic element strain ranges. The inner ceramic strain is maximum at steady state SLTO and is not increased by transient engine operation. The strains in the bond layer and the adjoining substrate layer are compressive when the inner substrate layer is in tension. The conclusion is that the ceremic outer layer strains are due to the linear expansion coefficient mismatch and temperature gradient and not a result of large substrate strains.

The maximum calculated outer ceramic layer elastic strains occurred during transient operation of the engine (Reference Figure 8). These maximum strains exceed the measured fracture strain level for plasma sprayed yttria stabilized zirconia based on P&WA conducted four point bending tests (Reference Figure 17). For stresses or strains that are not elastic or for conditions which exceed the brittle-ductile transition temperature these stress results do not apply.

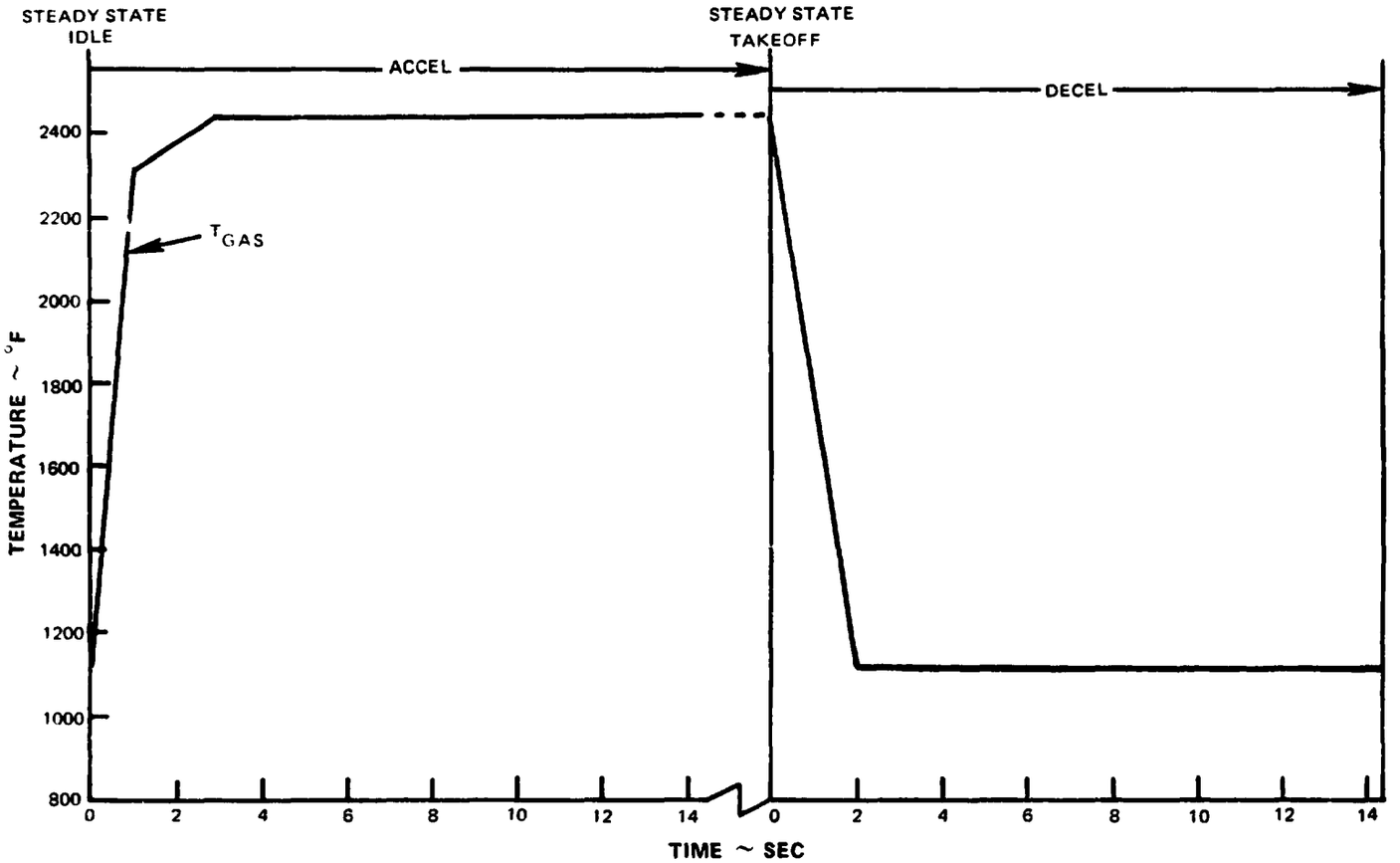

Figure 1 JT9D-7F Engine Endurance Cycle

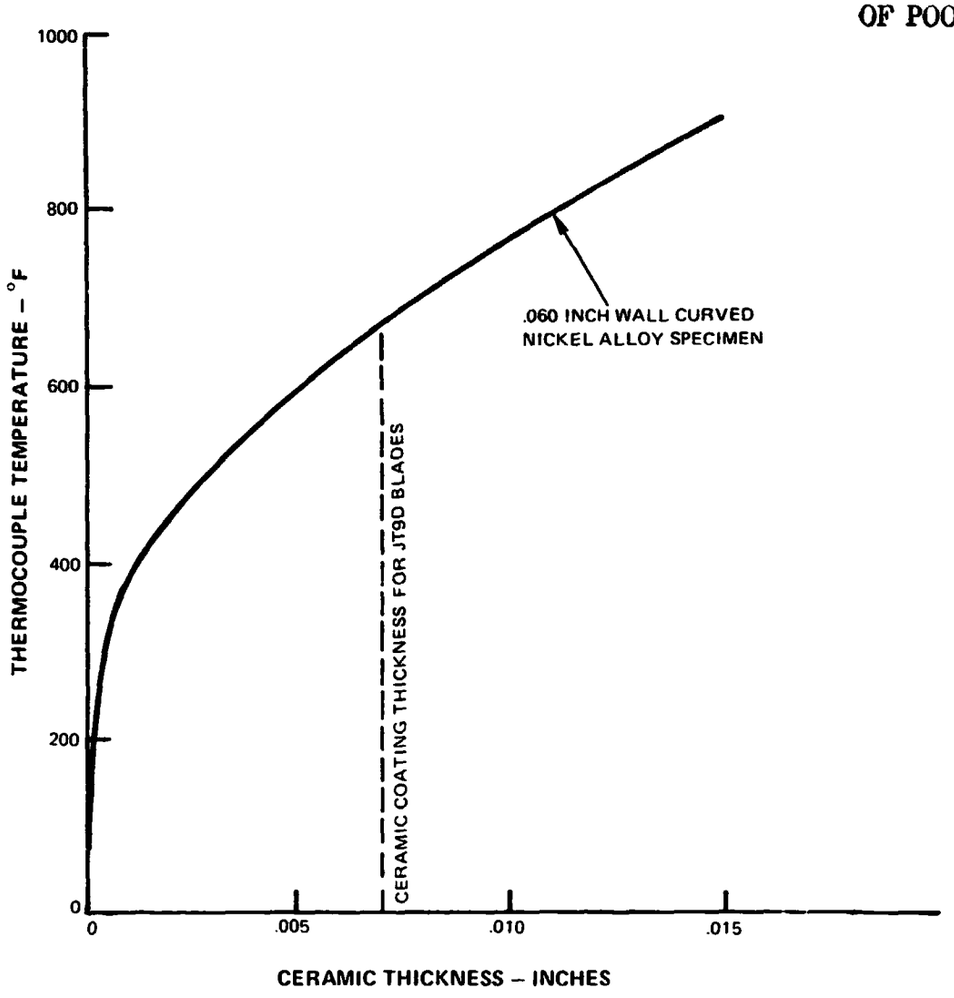

Figure 2 Temperature Response of Base Alloy Thermocouple During Ceramic Coating Application

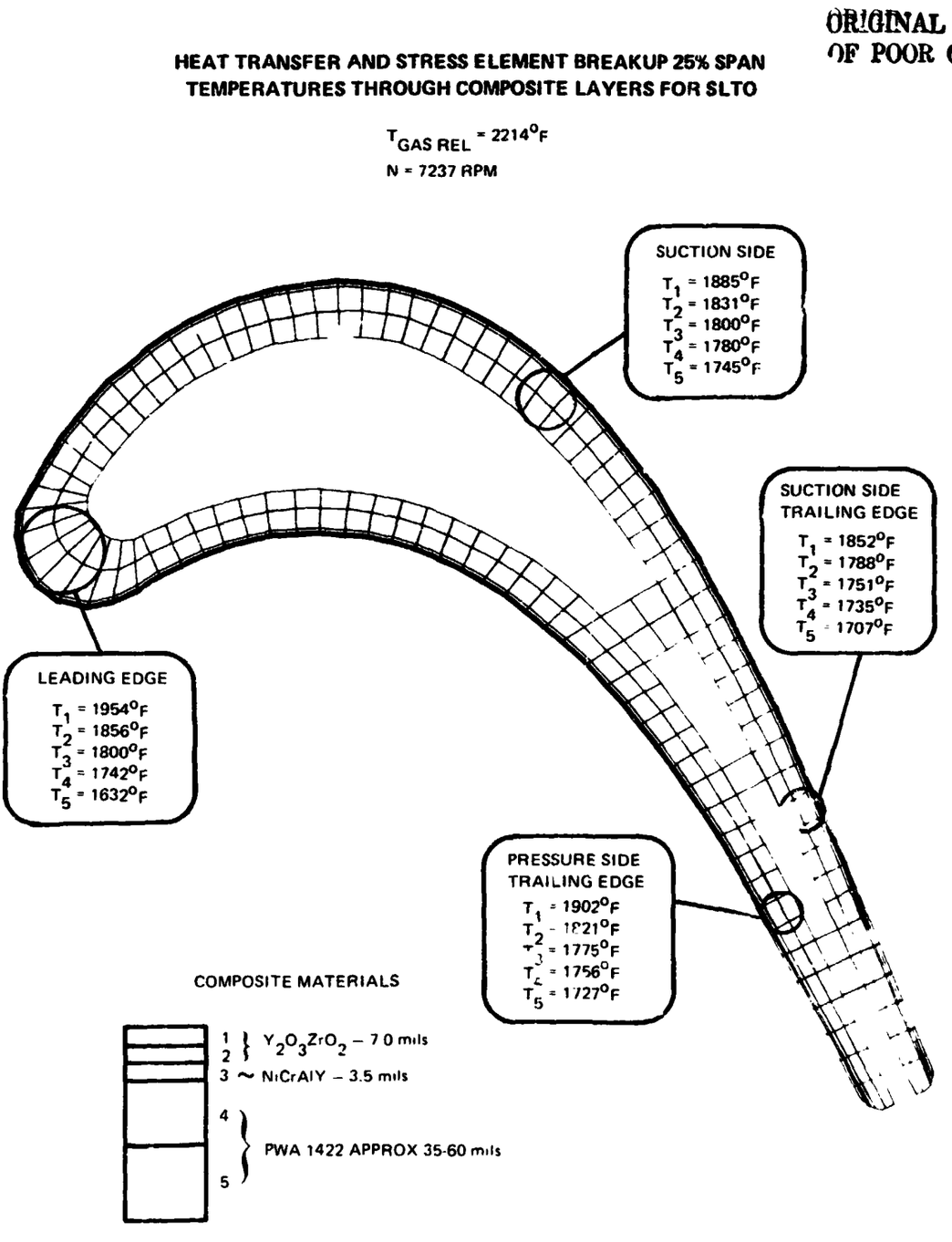

Figure 3 Heat Transfer and Stress Element Breakup at 25% Span Location. Temperatures are shown through composite layers for sea level takeoff condition.

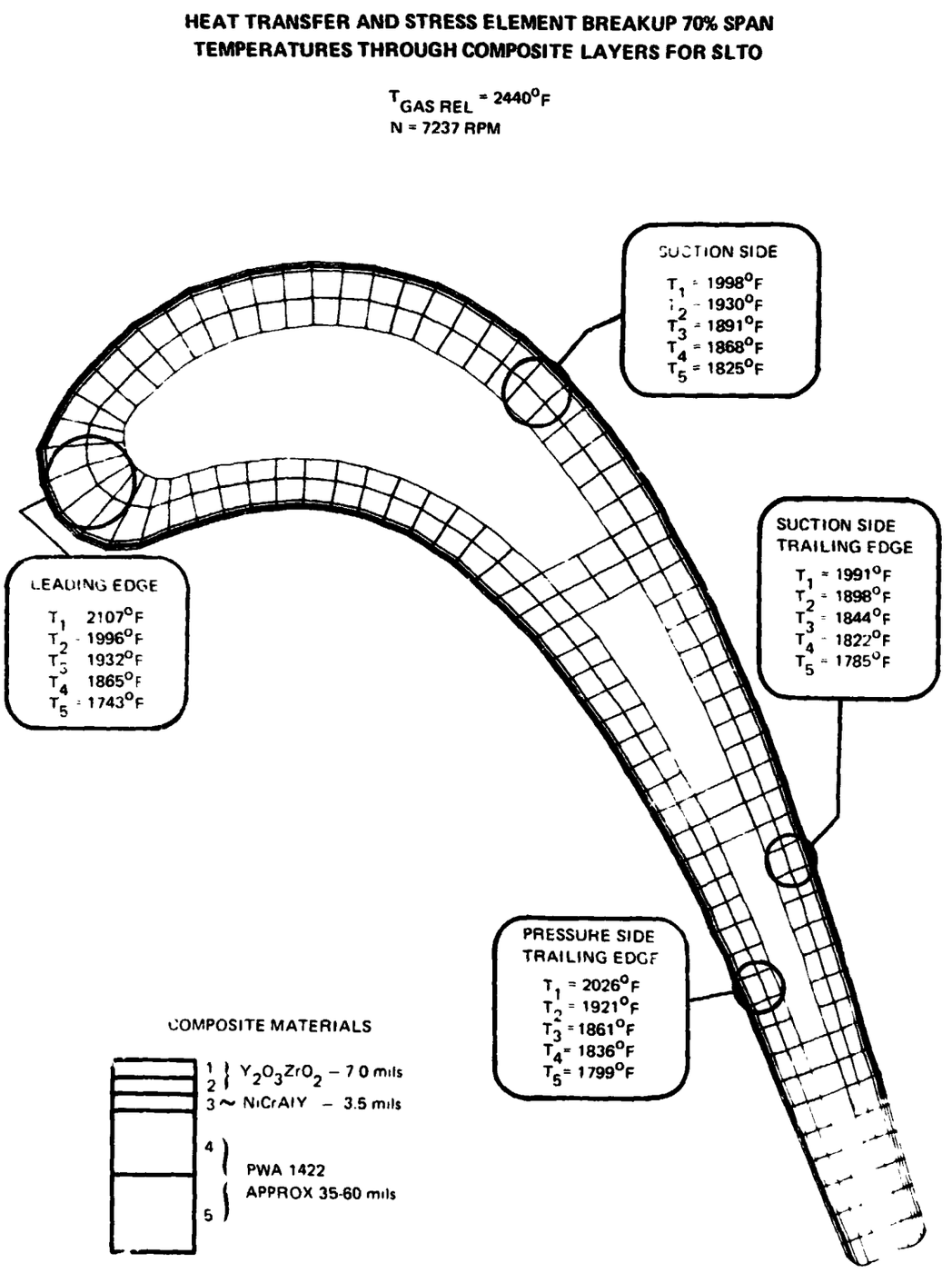

Figure 4 Heat Transfer and Stress Element Breakup at 70% Span Location. Temperatures are shown through composite layers for sea level takeoff condition.

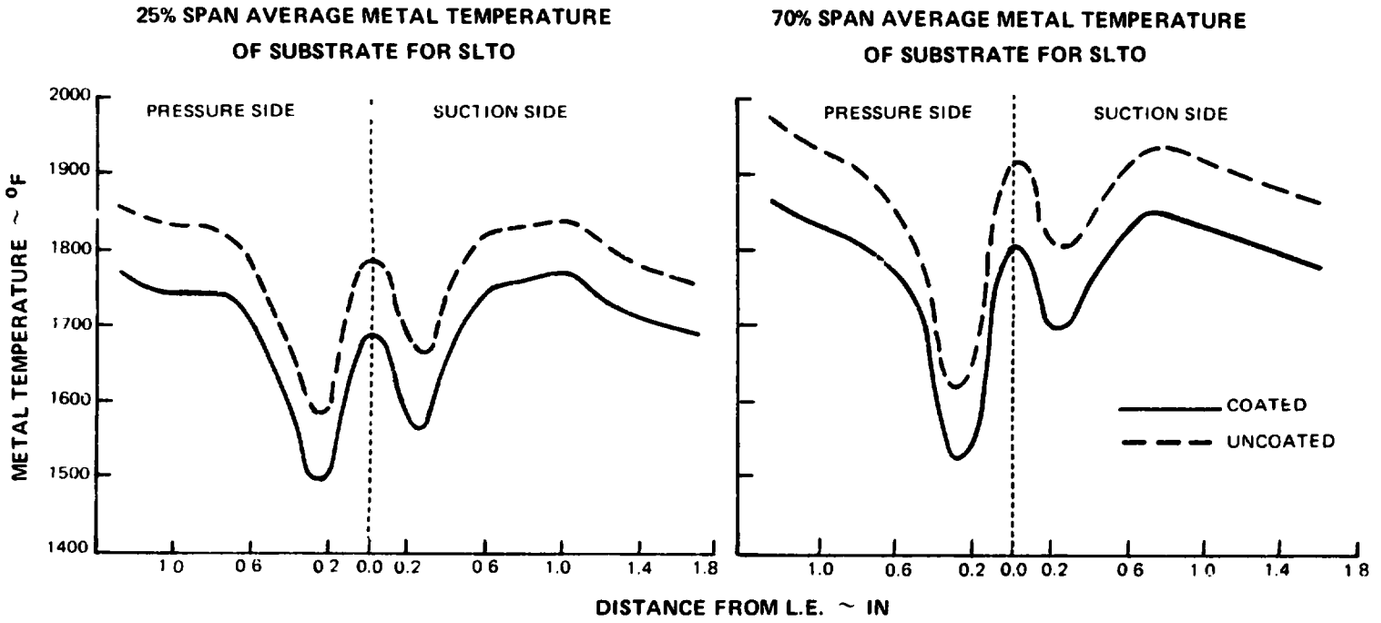

Figure 5 Average Metal Temperature of Substrate for Sea Level Takeoff Condition at Both 25% and 70% Span Location.

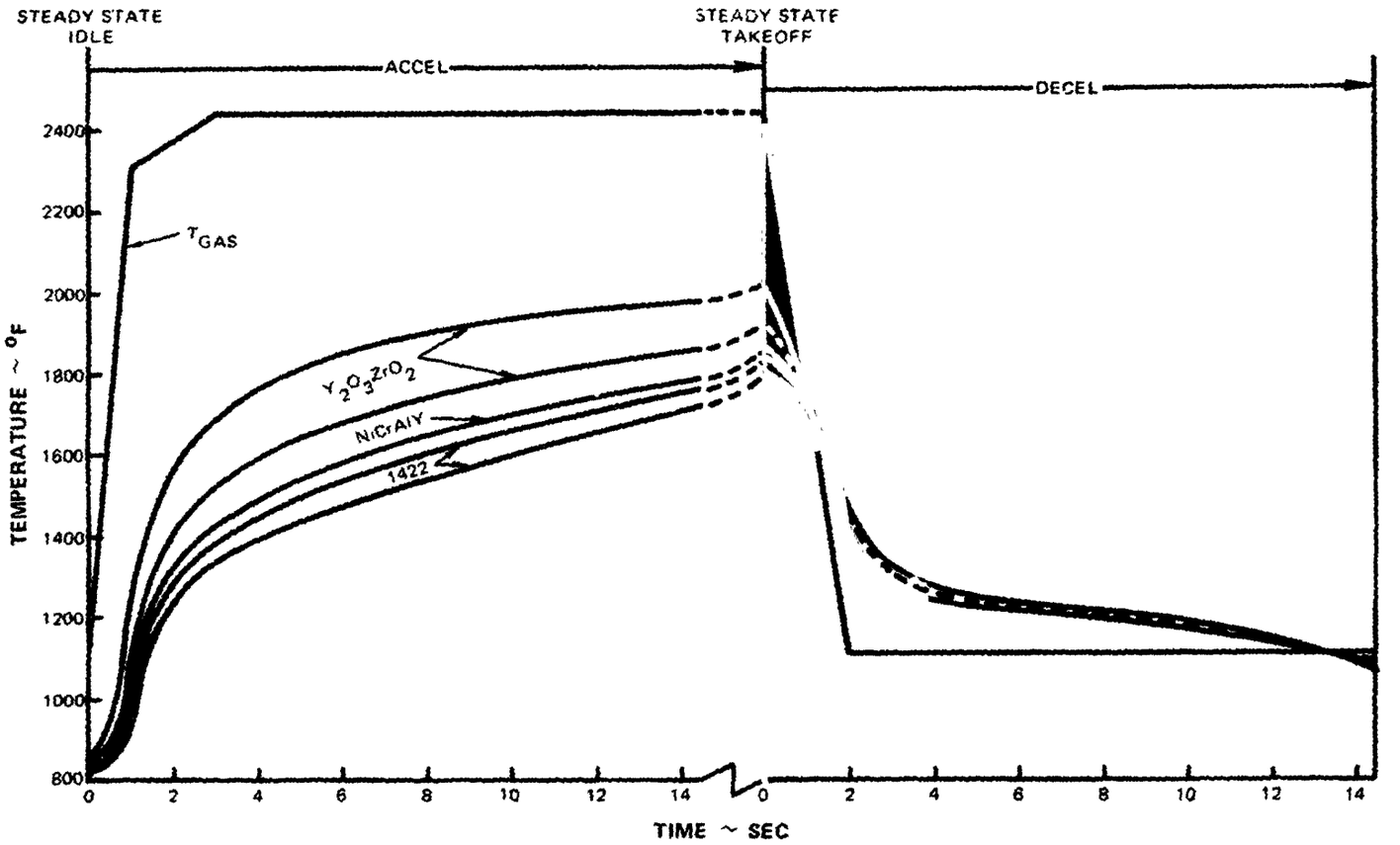

Figure 6 Temperature Response of Thermal Barrier Coating and Substrate at 70% Span Location, Pressure Side Trailing Edge

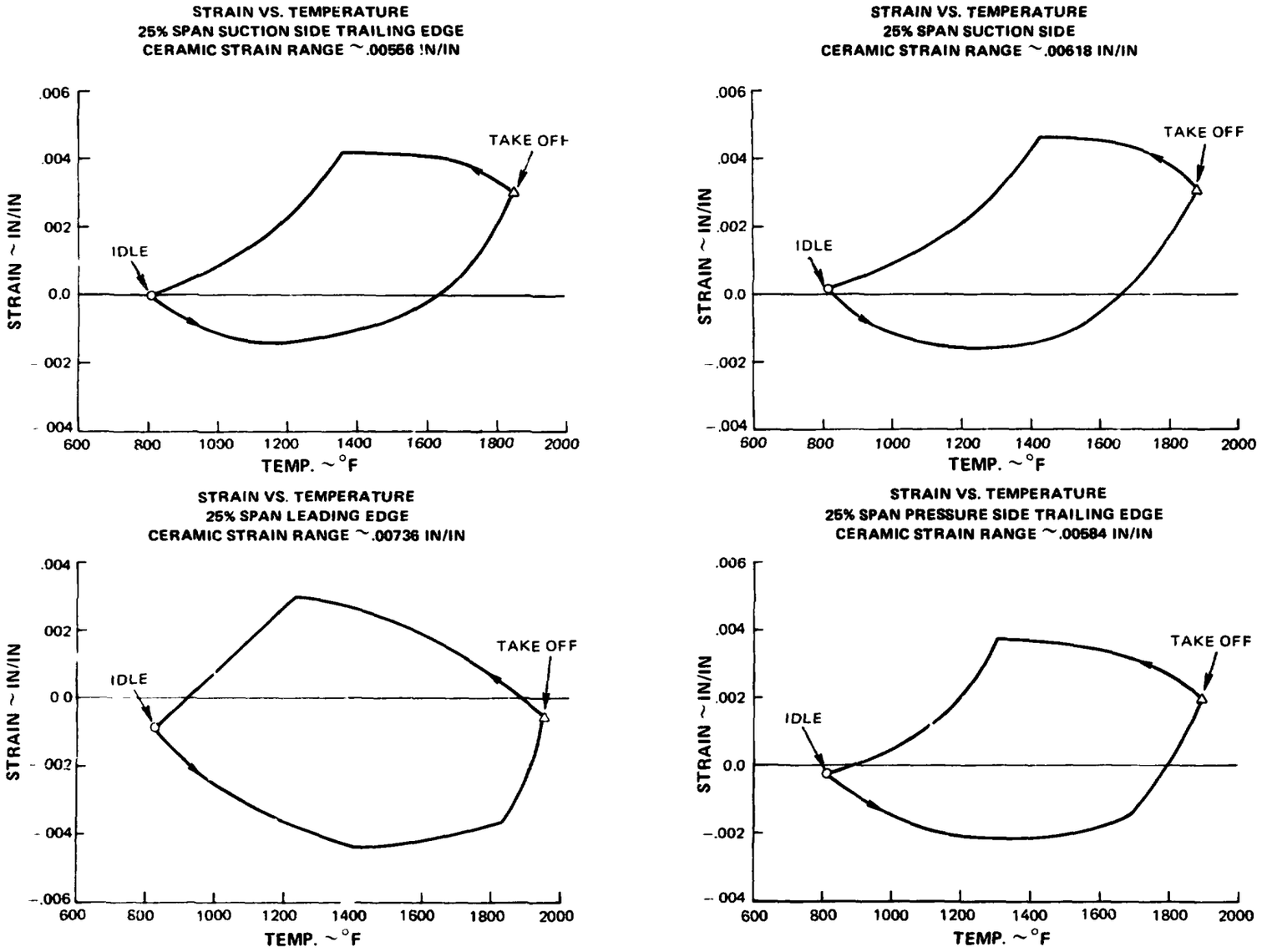

Figure 7 Ceramic Strain Versus Temperature in the Four Regions of Highest Strain (Reference Figure 3) at 25% Span Location

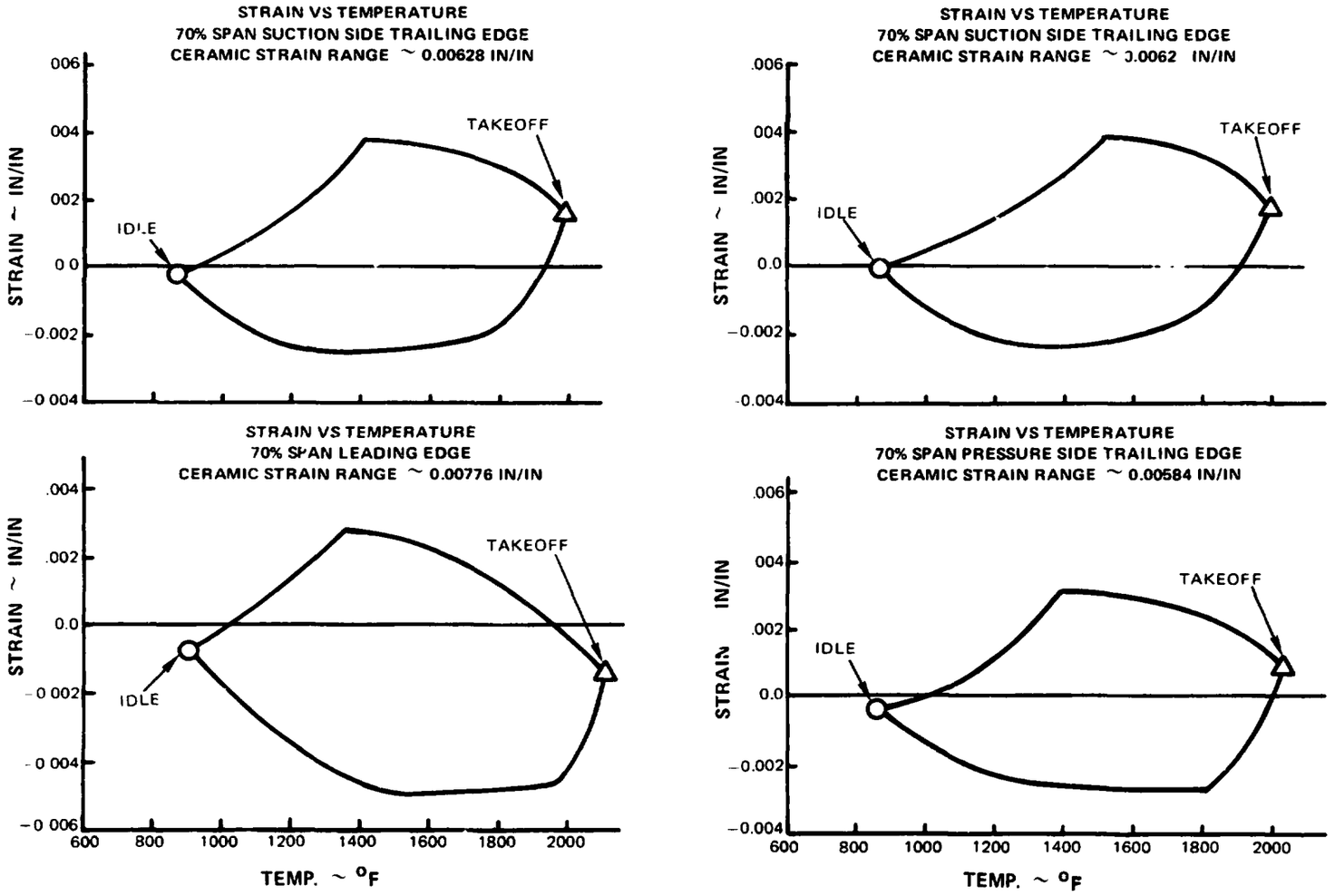

Figure 8 Ceramic Strain Versus Temperature in the Four Regions of Highest Strain (Reference Figure 3) at 70% Span Location

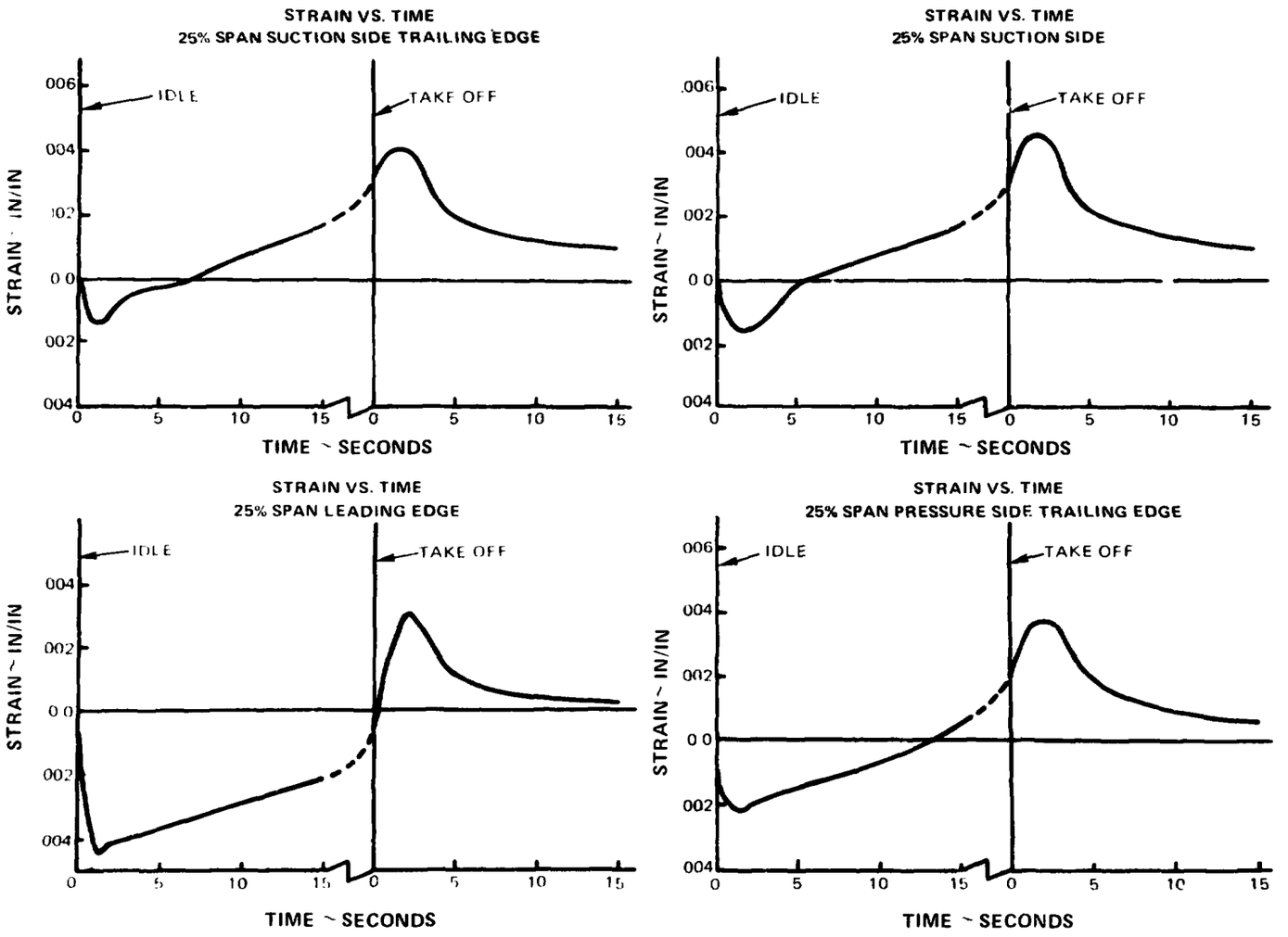

Figure 9 Ceramic Strain Versus Time in the Four Regions of Highest Strain (Reference Figure 3) at 25% Span Location

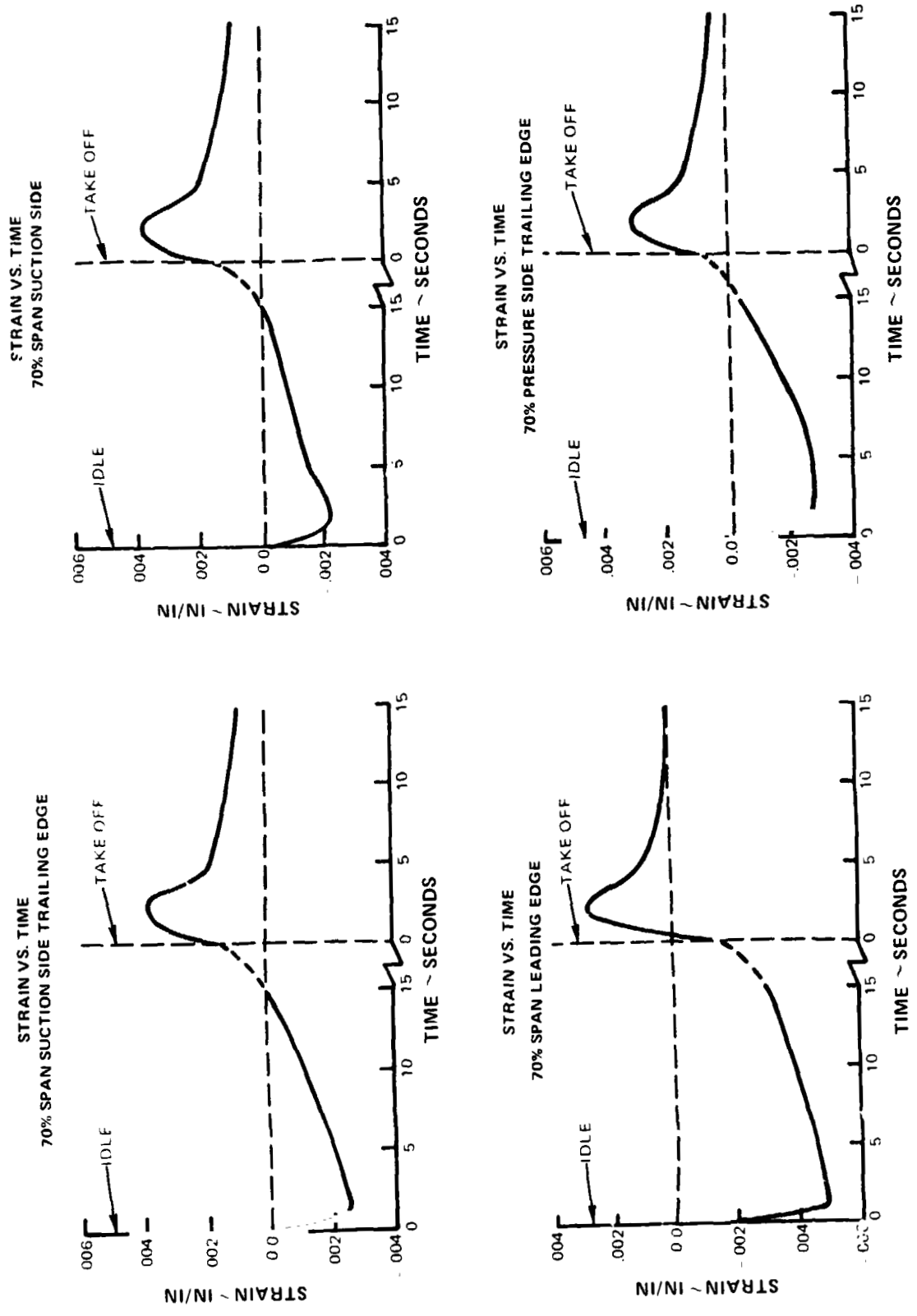

Figure 10 Ceramic Strain Versus Time in the Four Regions of Highest Strain (Reference Figure 3) at 70% Span Location

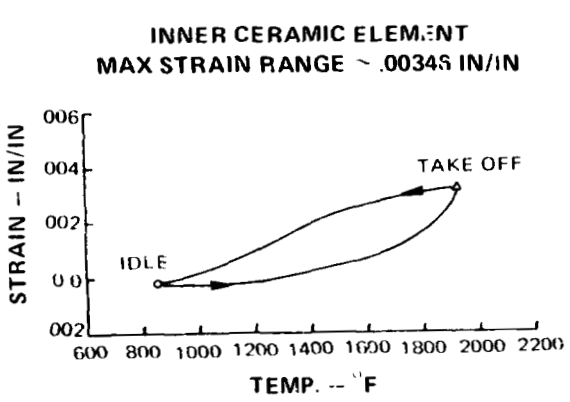

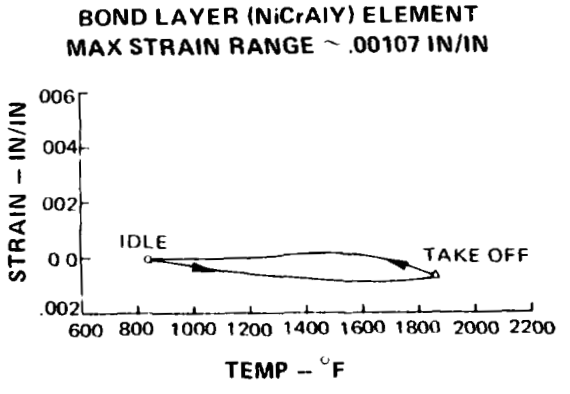

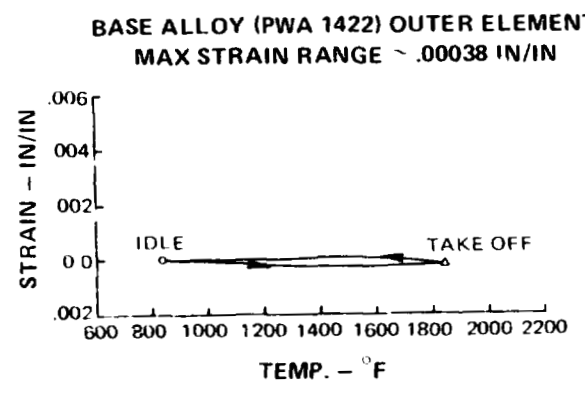

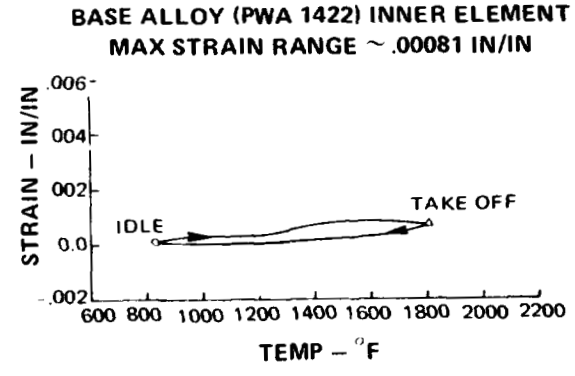

Figure 11 Strain Versus Temperature for Composite Elements Other Than Ceramic Surface Element, Shown at the Trailing Edge Pressure Side 70% Span Location

APPENDIX

REFERENCE TEMPERATURES

Figure 12 -- Effect of Reference Temperature On Strain Range

JT9D FIRST STAGE BOUNDARY CONDITIONS

Figure 13 -- Hot Gas Relative Temperature Along Blade Wall

Figure 14 -- Hot Gas Convective Film Coefficient Along Blade Wall

MATERIAL PROPERTIES

Figure 15 -- Thermal Conductivity and Modulus of Elasticity Versus Temperature

Figure 16 -- Specific Heat and Thermal Coefficient of Linear Expansion Versus Temperature, and Table of Material Density.

Figure 17 -- Ceramic Layer Fracture Strain

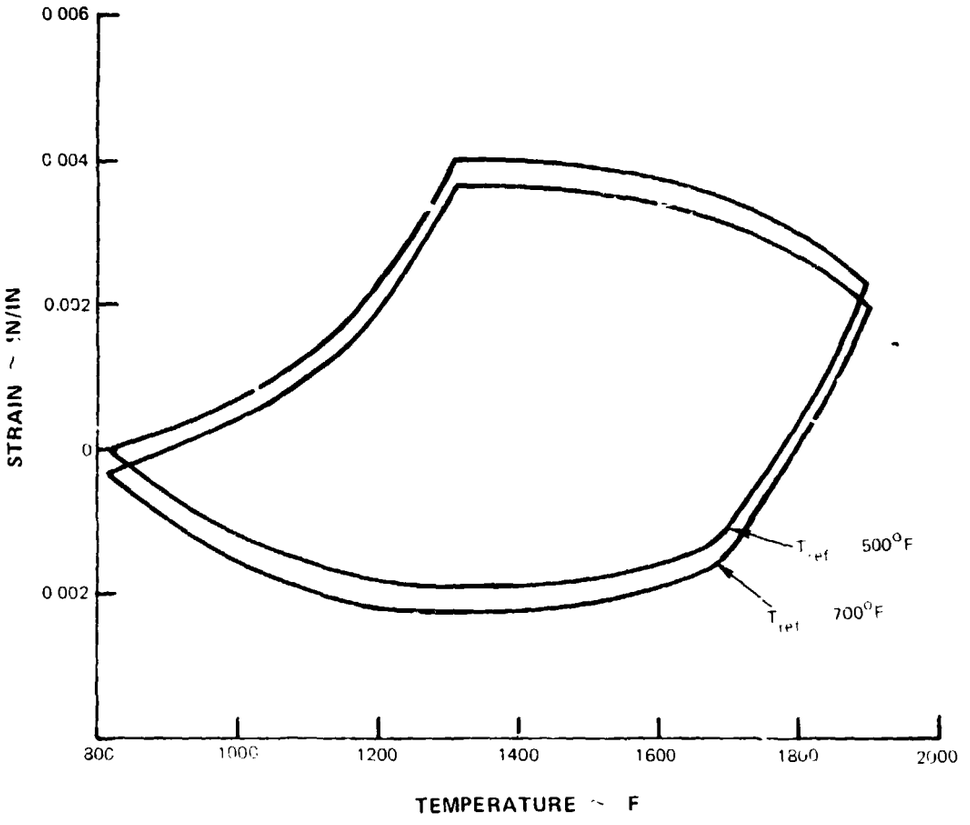

Figure 12 Effect of Reference Temperature on Strain Range

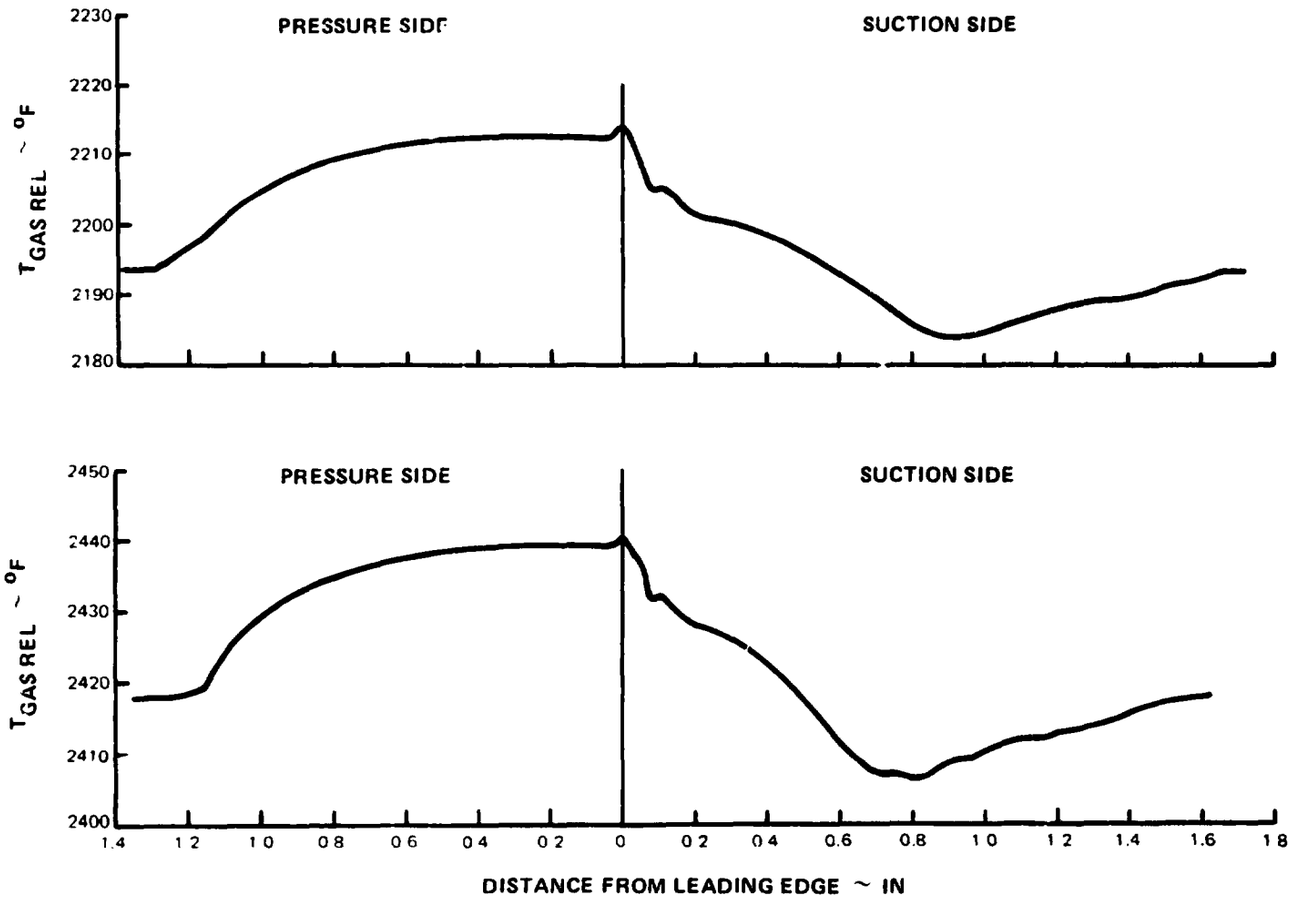

Figure 13 Relative Gas Temperature Versus Surface Distance at 25% and 70% Span Locations

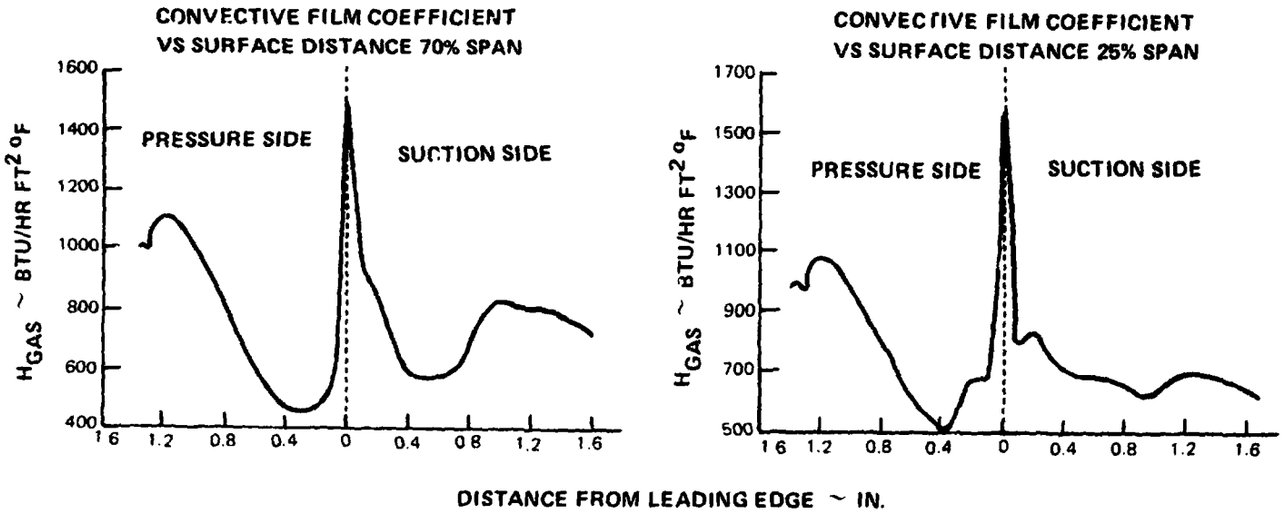

Figure 14 Convective Film Coefficient Versus Surface Distance at 25% and 70% Span Locations

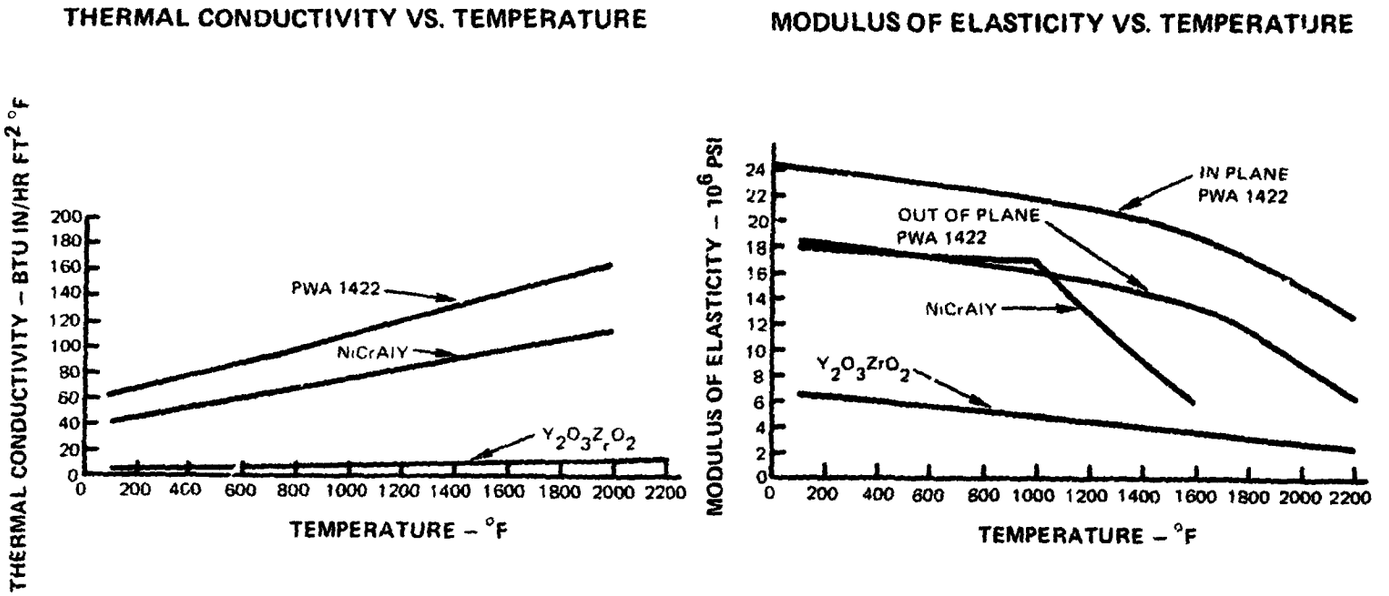

gure 15 Thermal Conductivity and Modulus of Elasticity Versus Temperature

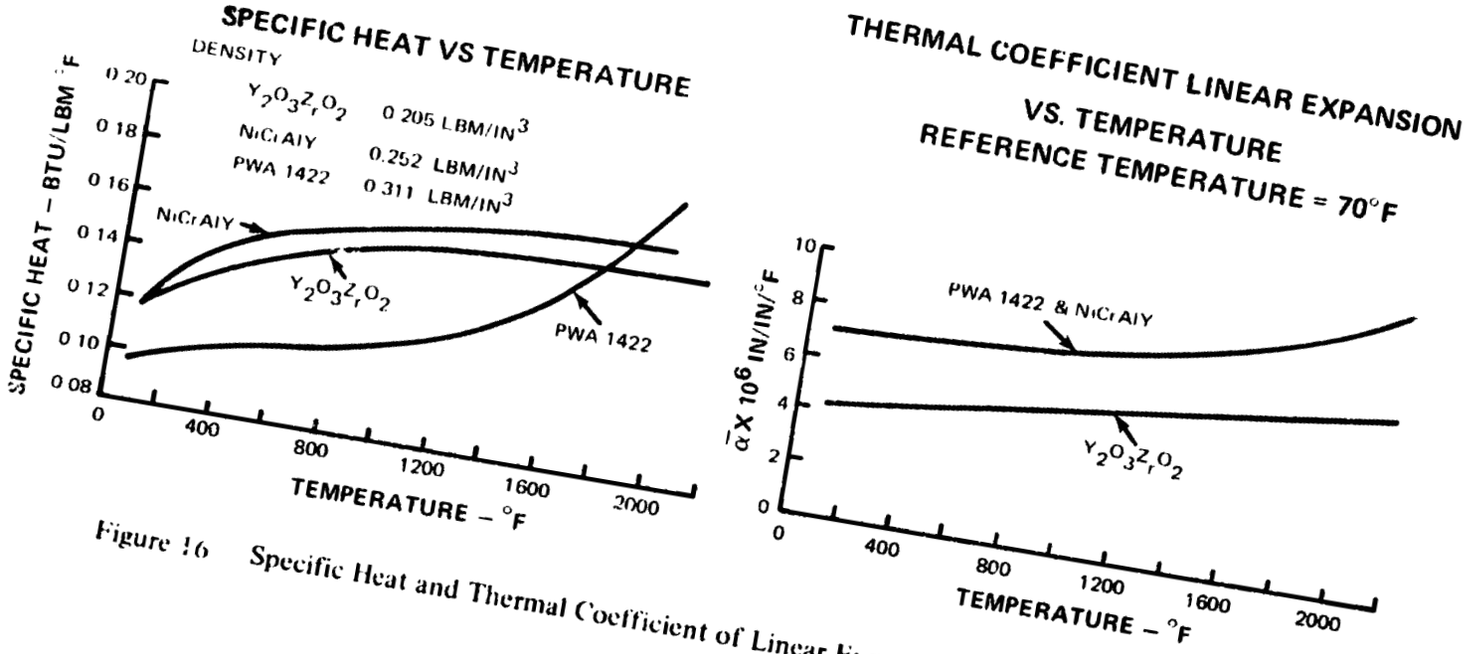

Figure 16 Specific Heat and Thermal Coefficient of Linear Expansion Versus Temperature

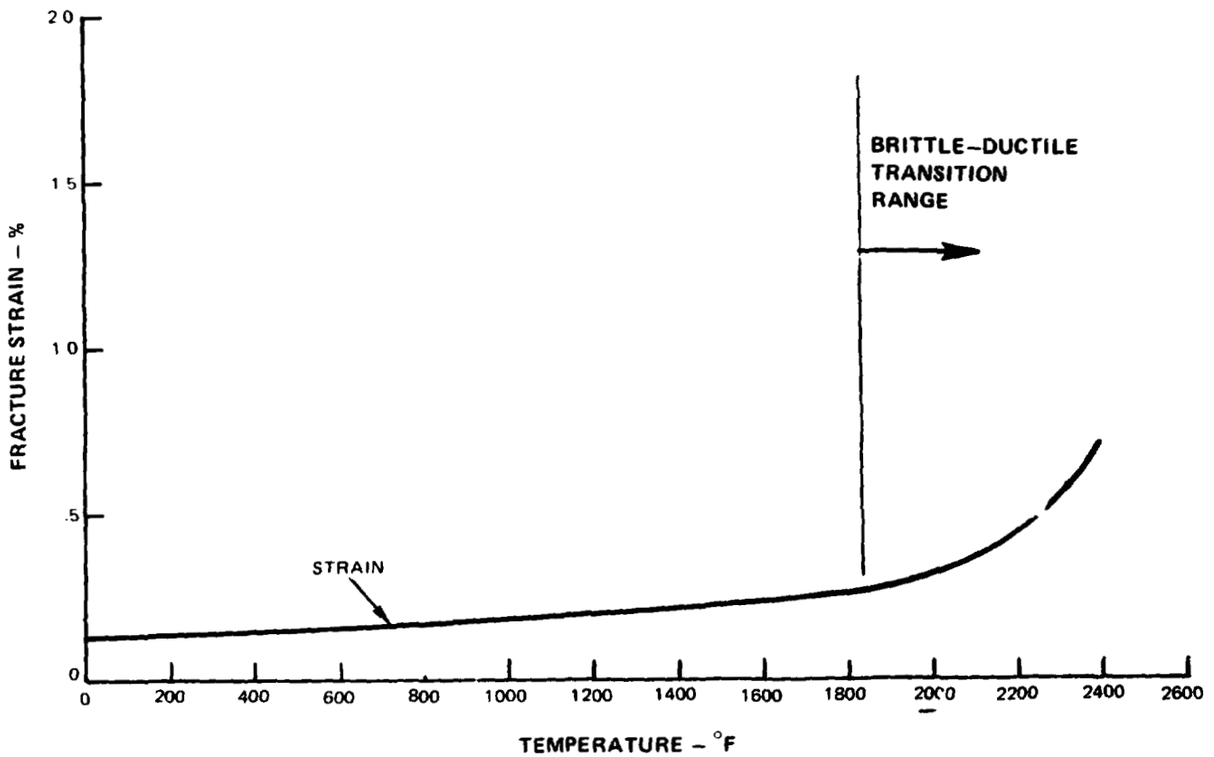

Figure 17 Ceramic Layer Fracture Strain ($Y_2O_3ZrO_2$)

10.0 REFERENCES

1. U. S. Patent No. 4,055,705 - F. Stecura and C. Liebert

2. Informal report to NASA from T. Strangman and B. Stoner, titled: "Evaluation of Thermal Barrier Coating Performance on Engine Tested JT9D-7F First Stage Turbine Blades", June 1977.